A Top-Down and Bottom-Up Diffusion Model of C_T^2 and C_Q^2 in the Entraining Convective Boundary Layer

C. W. FAIRALL

Department of Meteorology, The Pennsylvania State University, University Park, PA 16802

(Manuscript received 1 May 1986, in final form 10 October 1986)

ABSTRACT

A model of scalar structure function parameters in the entraining, convective boundary layer is developed based on a top-down and bottom-up diffusion approach. The behavior of the structure function parameters is obtained from the large eddy simulations of the scalar variance budget equations given by Moeng and Wyngaard. The conventional convective scaling formalism is augmented with an additional scaling parameter, R_c, which is the ratio of the entrainment flux of the scalar variable, C, to the surface flux. The model is compared to atmospheric measurements of the structure function parameters for temperature (C_T^2) and humidity (C_Q^2). Two types of comparisons are done: average profiles from several well known measurement campaigns (e.g., Minnesota and AMTEX) and individual profiles from twenty soundings by a light aircraft. The model appears to fit the C_Q^2 data better than it fits the C_T^2 data, particularly for the average profiles. There is a tendency for the model to underestimate the structure function parameters in the upper mixed-layer, particularly for C_T^2.

1. Introduction

Primarily spurred by interest in the effects of turbulence on the propagation of electromagnetic and acoustic radiation in the atmosphere (Tatarskii, 1962), the behavior of the scalar structure function parameters, C_T^2 and C_Q^2, has been intensely studied since the 1960s. The profiles of the structure function parameters have been well described in the surface-layer (Wyngaard et al., 1971) by Monin-Obukhov similarity theory. These results have been confirmed in a number of subsequent studies (e.g., Davidson et al., 1978; Kohsiek, 1982; Smith et al., 1983). Under unstable conditions, the surface layer expressions approach a free convection height dependence (Wyngaard, 1973) which is commonly referred to as the "$z^{-4/3}$" profile. In a study of convective mixed-layers, Kaimal et al. (1976) observed the free convection height dependence of the temperature structure function parameter up to 70% of the depth of the boundary layer. Quite similar results were obtained by Caughey and Palmer (1979). In a landmark paper, Wyngaard and LeMone (1980) showed that the strong peaks in C_T^2 and C_Q^2 typically observed at the top of the mixed-layer were caused by the entrainment of free tropospheric air into the boundary layer. Fairall (1984) extended the Wyngaard-LeMone model of interfacial-layer structure function parameters to include enhancement by wind shear at the inversion.

The final step in this process is to describe the structure function parameters in the height region between free convective behavior and the inversion. As it turns out, the free convective behavior often does not extend to 70% of the mixed-layer as observed by Kaimal et al. Frisch and Ochs (1975) published aircraft measurements of C_T^2 that showed substantial deviations from $z^{-4/3}$ even at the lowest parts of the mixed layer. They expressed these deviations in terms of the function $G(z/z_i)$ which is equal to one when free convection behavior is obeyed (z is the altitude and z_i the height of the top of the boundary layer). They found the value of G increased monotonically as z/z_i increased. A number of subsequent experimental studies (Weill et al., 1980; Fairall et al., 1980; Dubosclard, 1982; Druilhet et al., 1983) have clearly demonstrated that G is not a universal function of z/z_i but must include at least one other variable. The most revealing work in this respect was done by Burk (1981) who used a second-order closure model to study the behavior of the scalar structure functions in the entraining convective boundary layer. While it is generally agreed that this increase in the scalar structure function parameters is due to entrainment, present scaling parameterizations of C_T^2 and C_Q^2 in the upper PBL are essentially empirical curves fit to various sets of data (e.g., Frisch and Ochs, 1975).

In this paper I will present a semi-empirical similarity model for C_T^2 and C_Q^2 which is applicable to the entire mixed-layer. The effects of entrainment are included naturally because the model is based on the top-down (entrainment) and bottom-up (surface flux) diffusion formalism developed by Wyngaard and Brost (1984). One of the conclusions of the top-down and bottom-up diffusion approach is that the scalars are not well mixed and, therefore, the term "mixed-layer" is somewhat misleading. In the interest of maintaining consistency with the literature and in order to distinguish

it from the surface-layer, I will continue this imprecise terminology. The structure function parameters are obtained from the scalar dissipation rates, χ, using the well-known Corrsin relation and assuming the convective limit for the rate of dissipation of turbulent kinetic energy, ϵ,

$$C_c^2 = 1.6\epsilon^{-1/3}\chi_c \approx 2.3\chi_c z_i^{1/3}/W_* \tag{1}$$

where c = temperature (T) or absolute humidity (Q), and W_* is the convective scaling velocity (Kaimal et al., 1976). As in the inversion-layer theory (Wyngaard and LeMone, 1980), the scalar dissipation rates are obtained from the scalar variance budget equation. Here (see section 2), however, the approach is to write the variance, $\overline{c^2}$, as the sum of three components (Moeng and Wyngaard, 1984)

$$\overline{c^2} = \overline{c_b^2} + \overline{c_t^2} + 2\overline{c_t c_b} \tag{2}$$

where the subscript t refers to top-down and b refers to bottom-up. Thus, three budget equations must be written, yielding three dissipation rates which are summed to give χ

$$\chi = \chi_b + \chi_t + 2\chi_{tb}. \tag{3}$$

Parameterizations for the individual terms of the variance budget equation are based on the large eddy simulation results for the vertical gradients of the mean quantities (Wyngaard and Brost, 1984) and variance budget (Moeng and Wyngaard, 1984). This process is described in section 3.

The model developed in section 3 describes the profile of the structure function parameter, C_c^2, in the convective mixed layer. In addition to the standard mixed-layer scaling parameters, an additional scaling parameter (the ratio of the entrainment flux to the surface flux) is introduced. Relaxation of the restriction of the model to the pure convective form of the bottom-up term and a discussion of the use of an explicit form for the entrainment flux is described in section 4. In section 5, the model is compared with selected set of data.

2. Background

The vertical diffusion of a passive, conservative scalar through the convective PBL can be considered as the superposition of top-down and bottom-up components driven by the scalar fluxes at the mixed-layer top and bottom (see the original paper by Wyngaard and Brost, 1984, for details). For example, the vertical flux of the variable, C, can be represented as

$$\overline{cw} = \overline{cw}_s(1-\zeta) + \overline{cw}_i\zeta \tag{4}$$

where c and w denote turbulent fluctuations of C and vertical velocity, $\zeta = z/z_i$, s denotes the surface value, i denotes the interfacial value and the overbar represents the ensemble average. Alternatively, (4) can be expressed

$$\overline{cw} = \overline{cw}_s e_b + \overline{cw}_i e_t = \overline{c_b w} + \overline{c_t w} \tag{5}$$

where $e_b = (1-\zeta)$ is the bottom-up flux function and $e_t = \zeta$ is the top-down flux function. Similarly, the vertical gradient of the average of C can be written

$$\partial\bar{C}/\partial z = \partial\bar{C}_b/\partial z + \partial\bar{C}_t/\partial z \tag{6}$$

where

$$\partial\bar{C}_b/\partial z = (-\overline{cw}_s/W_* z_i)g_b \tag{7a}$$

$$\partial\bar{C}_t/\partial z = (-\overline{cw}_i/W_* z_i)g_t \tag{7b}$$

where $g_b = 0.4\zeta^{-3/2}$ and $g_t = 0.7(1-\zeta)^{-2}$ represent the bottom-up and top-down gradient functions using the notation of Moeng and Wyngaard (1984). In dimensionless form, the total gradient can be expressed

$$-(z_i/C_*)\partial\bar{C}/\partial z = g_b(\zeta) + R_c g_t(\zeta) \tag{8}$$

where $C_* = \overline{cw}_s/W_*$ and $R_c = \overline{cw}_i/\overline{cw}_s$. In order to be consistent with the notation generally used in the literature, θ_* will denote C_* for temperature and Q_* will denote C_* for humidity.

The total variance of C is expressed as the variance of the sum of top-down and bottom-up components

$$\overline{c^2} = \overline{(c_b + c_t)^2} = \overline{c_b^2} + \overline{c_t^2} + 2\overline{c_t c_b}. \tag{9}$$

Following Moeng and Wyngaard (1984), we write a variance budget equation for each component

$$\partial\overline{c_b^2}/\partial t = -2\overline{c_b w}\frac{\partial\overline{C_b}}{\partial z} - \frac{\partial}{\partial z}(\overline{c_b^2 w}) - \chi_b \tag{10a}$$

$$\partial\overline{c_t^2}/\partial t = -2\overline{c_t w}\frac{\partial\overline{C_t}}{\partial z} - \frac{\partial}{\partial z}(\overline{c_t^2 w}) - \chi_t \tag{10b}$$

$$\partial\overline{c_t c_b}/\partial t = -\left(\overline{c_t w}\frac{\partial\overline{C_b}}{\partial z} + \overline{c_b w}\frac{\partial\overline{C_t}}{\partial z}\right) - \frac{\partial}{\partial z}(\overline{c_t c_b w}) - \chi_{tb}. \tag{10c}$$

Assuming that the time derivative term can be neglected, then each dissipation is the sum of a gradient production term, M, and a transport term, T,

$$\chi_b = M_b + T_b \tag{11a}$$

$$\chi_t = M_t + T_t \tag{11b}$$

$$\chi_{tb} = M_{tb} + T_{tb} \tag{11c}$$

where the first term on the right-hand side of Eq. (10a) is M_b, the second term is T_b, etc.

The structure function parameter equations are obtained by combining the Corrsin [Eq. (1)] relation with the convective limit form of the rate of dissipation of turbulent kinetic energy (Wyngaard and LeMone, 1980)

$$\epsilon^{1/3} \rightarrow 0.7 W_*/z_i^{1/3} \tag{12}$$

which yields the dimensionless relation

$$\hat{C}_c^2 = z_i^{2/3} C_c^2 / C_*^2 = 2.3\hat{\chi}_c \tag{13}$$

where the caret denotes normalization by convective mixed-layer scaling parameters and $\hat{\chi} = z_i\chi/(W_* C_*^2)$. When the effects of entrainment are negligible (as described in section 1), then the structure function parameters will obey the convective form

$$\hat{C}_c^2 = A_c \zeta^{-4/3} \tag{14}$$

where $A_T = 2.67$ and $A_Q = 1.9$. The values of A_T and A_Q are uncertain by about 30% (see Wyngaard and LeMone, 1980).

3. Top-down, bottom-up dissipation functions

The combination mixed-layer and top-down, bottom up similarity forms for the dissipation terms [as in Eq. (11)] are developed from the variance budget relations [Eq. (10)] by evaulating the individual terms using: 1) existing top-down, bottom-up relations, 2) the results of large eddy simulations from Moeng and Wyngaard (1984), and 3) arguments about the convective limit form of the bottom-up component. First the dissipation is written in normalized form

$$\chi = (W_* C_*^2/z_i)\hat{\chi} = (W_* C_*^2/z_i)(\tilde{\chi}_b + \tilde{\chi}_t R_c^2 + 2\tilde{\chi}_{tb} R_c) \tag{15}$$

where the individual components obey the normalized form of Eq. (11). For example,

$$\tilde{\chi}_b = \tilde{M}_b + \tilde{T}_b \tag{16}$$

and so on. The tilde denotes top-down, bottom-up normalization as defined by Moeng and Wyngaard (1984).

a. The gradient production terms

The gradient production terms are simply combinations of the flux expression [(Eq. (5)] and the gradient expression [Eq. (7)]. In normalized form they are

$$\tilde{M}_b = 2e_b g_b = 0.8(1-\zeta)\zeta^{-3/2} \tag{17a}$$

$$\tilde{M}_t = 2e_t g_t = 1.4\zeta(1-\zeta)^{-2} \tag{17b}$$

$$\tilde{M}_{tb} = (e_t g_b + e_b g_t) = [0.4\zeta^{-1/2} + 0.7(1-\zeta)^{-1}] \tag{17c}$$

These functions (recall that they are based on large eddy simulations of flux and gradient profiles) compare favorably with the large eddy simulation scalar variance calculations of Moeng and Wyngaard (1984) and shown in their Fig. 9. The top-down term is in very good agreement. The bottom-up term disagrees slightly in the upper part of the PBL where it is quite small but does not become negative as in the large eddy simulations. The cross term is also in good agreement except for $\zeta > 0.9$, where the large eddy simulations become negative and increase in magnitude.

b. The transport terms

Unlike the gradient production terms, the transport terms cannot be derived from pre-existing expressions. In this case, the large eddy simulations of Moeng and Wyngaard are used. Rather than use complex fits to the exact curves shown in their Fig. 9, very simple expressions were used that approximated their results. This approach was selected because the generality of the large eddy simulations is unknown and the "imbalance" term represents a potential source of uncertainty in any of their functions. Two of the functions were rather easily approximated by assuming that one-third of the local production was transported away:

$$\tilde{T}_t = -(1/3)\tilde{M}_t + 3 \tag{18a}$$

$$\tilde{T}_{tb} = -(1/3)\tilde{M}_{tb}. \tag{18b}$$

In the case of the top-down term it was necessary to add a constant to agree with the simulations in the lower half of the PBL. When all three components are considered, transport will be a gain below $0.8z_i$.

Rather than attempting to curve fit the bottom-up transport function to the eddy simulation results, we require that the bottom-up dissipation (the sum of transport and gradient production) obey the free convection limit [Eqs. (14) and (15)]

$$2.3(\tilde{M}_b + \tilde{T}_b) = A_c \zeta^{-4/3}. \tag{19}$$

This is logical since the convective limit is a purely surface effect (i.e., bottom-up) and convenient since it ensures that the solution will have the proper behavior in the lower PBL. This yields an expression for $\tilde{T}_b$ [through Eqs. (17a) and (19)] that very poorly approximates the large eddy simulations. The reason is that the large eddy simulations underestimate the dissipation and variances (see the discussion in section 6).

c. Structure function parameters

Combining the gradient production and transport terms yields relations for the individual dissipation terms

$$\tilde{\chi}_b = (A_c/2.3)\zeta^{-4/3} \tag{20a}$$

$$\tilde{\chi}_{tb} = \frac{2}{3}\tilde{M}_{tb} \tag{20b}$$

$$\tilde{\chi}_t = \frac{2}{3}\tilde{M}_t + 3 \tag{20c}$$

which, combined with Eqs. (13) and (15) gives the result for the structure function parameter

$$C_c^2 z_i^{2/3}/C_*^2 = A_c\zeta^{-4/3} + 2.3\left[\frac{4}{3}\tilde{M}_{tb}R_c + \left(\frac{2}{3}\tilde{M}_t + 3\right)R_c^2\right] \tag{21}$$

where $\tilde{M}_t$ and $\tilde{M}_{tb}$ are obtained from Eqs. (17b) and (17c). Writing this in a more simplified form,

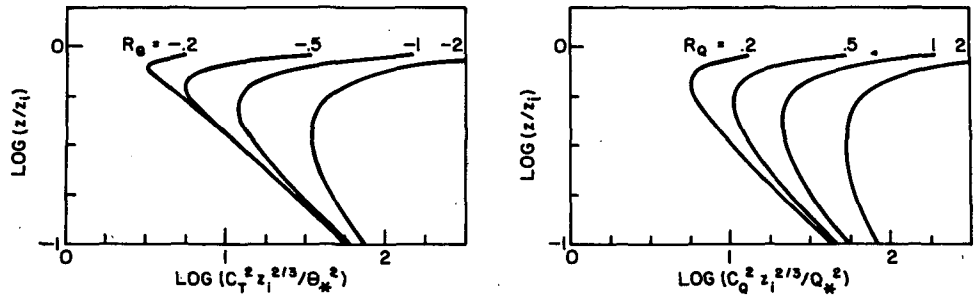

FIG. 1. Normalized profiles of structure function parameters based on the pure convection model expressions for typical values of R_c (indicated at the top of each curve). On the left is the temperature structure function profile and on the right is the humidity structure function profile.

$$C_c^2 = C_*^2 z_i^{-2/3}[h_b(\zeta) + R_c h_{tb}(\zeta) + R_c^2 h_t(\zeta)] \quad (22)$$

with the functions defined by

$$h_b(\zeta) = A_c \zeta^{-4/3} \quad (23a)$$

$$h_{tb}(\zeta) = 2.15[(1-\zeta)^{-1} + 0.57\zeta^{-1/2}] \quad (23b)$$

$$h_t(\zeta) = 7 + 2.15\zeta(1-\zeta)^{-2}. \quad (23c)$$

d. Surface-layer extension

The functions developed above are for the convective mixed-layer and are expected to have application in the region $0.1 < \zeta < 0.9$. Furthermore, the convective conditions used in this derivation [e.g., Eq. (12)] are often defined by the limits $z_i/(-L) > 10$, where L is the Monin-Obukhov length. It is straightforward to extend these results closer to the surface by modifying the bottom-up function, $h_b(\zeta)$, to be consistent with the surface layer scaling expression of Wyngaard et al., (1971):

$$h_b(\zeta) = 3.7A_c\zeta^{-2/3}[z_i/(-L)]^{2/3}(1-7z/L)^{-2/3}. \quad (24)$$

The advantage of this form is that it is valid regardless of the validity of Eq. (12) or conditions on $z_i/(-L)$. The forms of h_t and h_{tb} were obtained in convective conditions and cannot be expected to apply near the surface, but these terms are negligible for $\zeta < 0.1$ for typical values of R_c.

Sample profiles for the "pure convective" case [Eq. (23)] for temperature and humidity structure function parameters are shown in Fig. 1. The curves are shown for selected values of R_c (negative for temperature and positive for humidity) that are deemed to cover a range of typical atmospheric values (see, also, Moeng and Wyngaard, 1984). Qualitatively, these curves are very similar to the range of atmospheric observations presented by Wyngaard and Lemone, 1980 (see their Figs. 2 and 4). Notice that the temperature and humidity curves are not greatly different for the same values of the magnitude of R_c (thus, the top-bottom cross term tends to be less important). This implies that the significant differences in the shape of the normalized structure function profiles often observed in the atmosphere are primarily due to differences in the magnitudes of R_c for temperature and humidity. Similarly, sample profiles for the "surface layer" case (Eq. 24) are shown in Fig. 2. Here fixed values of R_c and z_i have been selected so the curves show the effect of changing surface layer stability. Obviously, many more combi-

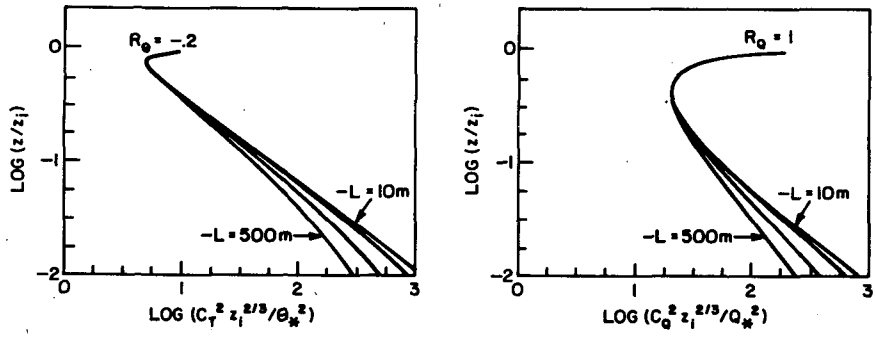

FIG. 2. Normalized profiles of structure function parameters based on the model including the surface-layer behavior [Eq. (24) rather than Eq. (23a)]. On the left is the temperature structure function profile and on the right is the humidity structure function profile. In each case R_c is fixed at a typical value and $-z_i$ at 1000 m; a separate curve is plotted for various values of $-L$ (10 m, 100 m, 200 m, and 500 m).

nations of variables are possible but the expressions are easily calculated by the interested reader.

e. Miscellaneous comments

A reviewer of this manuscript (Burk, private communication, 1986) has pointed out that the complex derivation of Eq. (23) from the scalar variance budget equations is not necessary. Moeng and Wyngaard (1984) define a dissipation time scale, τ, such that

$$\hat{X}_c = \hat{\overline{c^2}}/\hat{\tau}, \tag{25}$$

where

$$\hat{\tau} = \tau W_*/z_i.$$

Thus, by using Eq. (13) the structure functions can be obtained simply as

$$\hat{C}_c^2 = 2.3\hat{\overline{c^2}}/\hat{\tau} \tag{26}$$

Moeng and Wyngaard have provided a parameterization for $\hat{\overline{c^2}}$

$$\hat{\overline{c^2}} = f_b + 2f_{tb}R_c + f_t R_c^2 \tag{27}$$

where f_b, f_{tb} and f_t are dimensionless functions of ζ. Clearly, Eqs. (26) and (27) can be combined to yield

$$\hat{C}_c^2 = 2.3[f_b/\hat{\tau}_b + 2(f_{tb}/\hat{\tau}_{tb})R_c + (f_t/\hat{\tau}_t)R_c^2]. \tag{28}$$

A simple approximation for the $\hat{\tau}$ terms can be taken from Moeng and Wyngaard's Fig. 10 and a final expression developed that is quite similar to Eq. (22).

This approach has the obvious advantage that Moeng and Wyngaard have done all of the work in computing the empirical functions. Since the data input is based on the same large eddy simulations, either approach should yield about the same final result (they do). The major advantage of the original approach is a clear indication of the importance of the internal processes (transport and gradient production) that are contributing to the structure functions. Incidentally, the second approach allows us to easily develop a parameterization for the temperature humidity structure function parameter, C_{Tq}, (Wyngaard and LeMone, 1980)

$$\hat{C}_{Tq} = 2.3\hat{\overline{\theta q}}/\hat{\tau}. \tag{29}$$

Following the same arguments as above yields the result

$$\hat{C}_{Tq} = 2.3[f_b/\hat{\tau}_b + (f_{tb}/\hat{\tau}_{tb})(R_\theta + R_q) + (f_t/\hat{\tau}_t)R_\theta R_q]. \tag{30}$$

4. Entrainment rate

The application of these equations requires knowledge of the surface fluxes of momentum, sensible heat, and latent heat (or, equivalently, the surface layer scaling parameters u_*, T_* and q_*) plus the height of the mixed-layer and the scalar fluxed at the inversion. The inversion fluxes are conventionally expressed in terms of the entrainment velocity, W_e, given by

$$\overline{cw}_i = -W_e \Delta C \tag{31}$$

where ΔC is the increase in the value of $\bar{C}$ across the inversion. At first this may appear to be negative progress since we have traded one unknown (the scalar flux at the inversion) for two unknowns (the interfacial jump plus the entrainment velocity). The point is that we wish to express the problem in terms of quantities that we are more likely to know (after all, it is considerably easier to measure the scalar structure function parameters themselves than the eddy covariances one km above the surface). In this regard, the entrainment velocity is obtained from an empirical model relating W_e to the parameters already specified. In the classic cloud-free, entraining convective boundary layer, this relation is most simply given by (Tennekes and Driedonks, 1981)

$$W_e \approx 0.2\overline{\theta w}_s/\Delta\theta. \tag{32}$$

This expression immediately leads to

$$R_\theta = -0.2. \tag{33}$$

Since the theory presented here is for cloud-free conditions, a discussion of cloud induced entrainment is unnecessary. However, even under cloud-free conditions, Eq. (32) may not account for all entrainment mechanisms active in the real atmosphere (e.g., see Tennekes and Driedonks, 1981). In the interest of consistency with the surface layer effects expressed in Eq. (24), the surface shear induced entrainment can be included with an additional term (Fairall, 1984)

$$W_e = 0.2(\overline{\theta w}_s + F_{sh})/\Delta\theta \tag{34}$$

where

$$F_{sh} = 8u_*^3/(gTz_i). \tag{35}$$

A bit of algebraic manipulation is sufficient to show that Eq. (33) can now be expressed

$$R_\theta = -0.2[1 + 3.2(-L/z_i)] \tag{36}$$

where the arithmetic factor 3.2 represents 8 times the von Karman constant. Sample curves for normalized C_T^2 are shown in Fig. 3 to illustrate the effect of decreasing inversion height at fixed values of surface layer stability. Notice that for typical daytime, overland convective conditions ($L = -10$ m) the curves (Fig. 3a) are virtually indistinguishable from the "pure convection" case while conditions more representative of a marine mixed-layer (Fig. 3b) show substantial influence from the lowering of the inversion.

5. Comparison with data

Two types of comparisons with atmospheric measurements will be made: 1) with data composited over many days of measurements and 2) specific profiles from aircraft soundings. In Fig. 4 the pure convective model [Eq. (23)] is overlain with the average normalized profile of C_T^2 from the Minnesota experiment

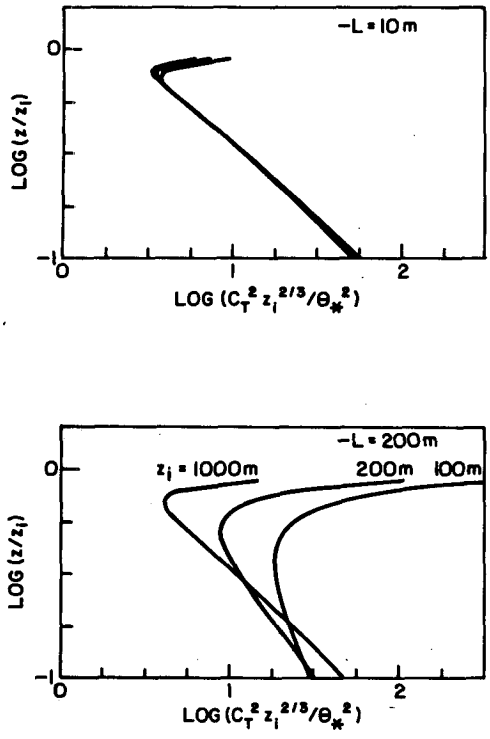

FIG. 3. Normalized profiles of temperature structure function parameter based on the model including surface-layer behavior and Eq. (36) for R_θ. The upper panel is for $-L$ = 10 m and the lower panel is for $-L$ = 200 m; a separate curve is plotted for various values of z_i (1000, 200 and 100 m).

(Kaimal et al., 1976). In this case it is known from the measurements that the average value of R_θ is -0.2. Also shown in Fig. 4 is a one-dimensional, second order closure result from Burk (1981). Notice that the measurements are always greater than the $\zeta^{-4/3}$ line but the model can be slightly less (this is the influence of the cross term, which is negative for temperature). In the case of the closure model results, this failing is associated with too weak *transport* of temperature variance in the formulation used by Burk (i.e., in the strongly bottom-up situation, the magnitude of C_T^2 in the vicinity of $z/z_i \sim 0.7$ is quite sensitive to the magnitude of the transport term). In Fig. 5 the model is compared with the average normalized profile of C_Q^2 from AMTEX (Wyngaard and LeMone, 1980). In this case the average value of R_Q is near 0.5. Moeng and Wyngaard (1984) used $R_Q = 0.5$ and $R_Q = 1.0$ to compare with average AMTEX data, so model curves for these values are indicated in Fig. 5. In Fig. 6 the model is overlain with the average normalized profile of C_Q^2 from Druilhet et al. (1983). Here C_Q^2 is not normalized with Q_* but with the scaling parameter Q_{**}

$$Q_{**} = \overline{qw}_i / W_* = R_Q Q_*. \tag{37}$$

Druilhet et al. (1983) chose this normalization because the surface moisture flux was negligible for their measurements (i.e., $Q_* \to 0$). This is a particularly interesting comparison because it isolates the top-down (i.e.,

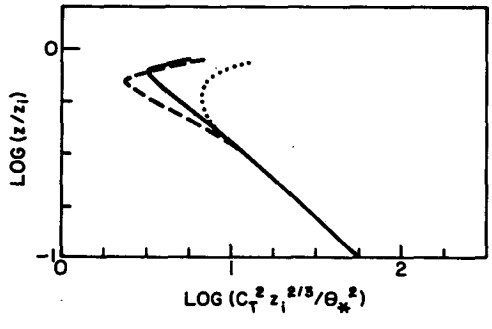

FIG. 4. Normalized profile of temperature structure function parameter. The solid line is the pure convection form of the model; the dashed line is the second-order closure result from Burk (1981); the dotted line is the average of measurements from the Minnesota experiment (Kaimal et al., 1976).

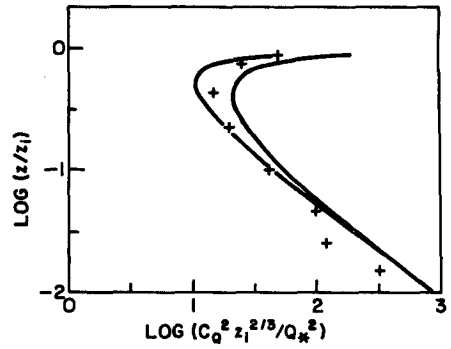

FIG. 5. Normalized profile of humidity structure function parameter. The crosses are average atmospheric measurements from the AMTEX experiment (Wyngaard and LeMone, 1980). The solid lines are the pure convection forms for the model with $R_Q = 0.5$ and $R_Q = 1.0$, values that are expected to bracket the AMTEX averages (Moeng and Wyngaard, 1984).

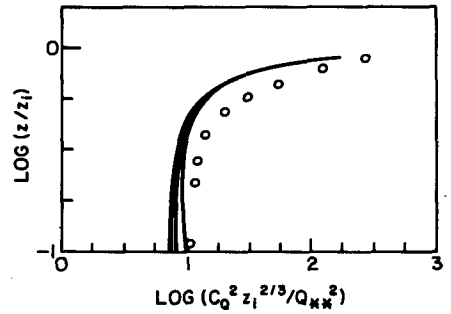

FIG. 6. Normalized profile of humidity structure function parameter. In this case C_Q^2 is normalized by the entrainment scaling parameter, Q_{**} [Eq. (37)]. The open circles are the average data points from Druilhet et al. (1983); the lines are the model expressions for various values of R_Q (near the bottom right to left, R_Q = 2, 5, 20 and 50).

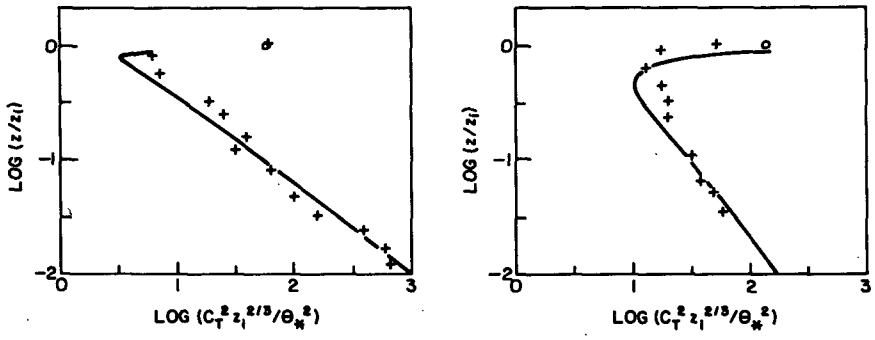

FIG. 7. Sample comparison of model expression with aircraft measurements of the temperature structure function parameter profiles in normalized form. The crosses are data points (two-minute, level flight average) and the solid line is the model including Eqs. (24) and (36). The highest data point is the average in the inversion and the open circle represents the Wyngaard and LeMone (1980) model value. In the left panel is data taken at White Sands, NM with an inversion height of 1900 m, $u_* = 0.47$ m s^{-1}, $T_* = -0.42$ K, $R_\theta = -0.22$ and $-L = 45$ m. In the right panel is data taken off the coast of California near Monterey with an inversion height of 230 m, $u_* = 0.41$ m s^{-1}, $T_* = -0.046$ K, $R_\theta = -0.90$ and $-L = 250$ m.

$R_Q \to \infty$) components of the theory and indicates very good agreement with a completely independent dataset where the scalar fluctuations are believed to be entirely due to entrainment.

A more detailed look at the theory is provided by comparison with another independent set of data obtained with an instrumented aircraft. A set of twenty fair-weather turbulence profiles were examined. Each profile included measurements of C_T^2 (made with fine resistance wire), ϵ (made with a hot wire anemometer), mean temperature and mean humidity. In some cases, measurements of C_Q^2 (made with a Lyman-α hygrometer) were also available. The surface scaling parameters (u_*, T_* and q_*) were determined from the Monin-Obukhov similarity relations for the structure functions and dissipation. Details on the instrumentation, measurement techniques and analysis methods can be found in previous papers (Fairall et al., 1980; Fairall, 1984). Figure 7 gives two examples of C_T^2 profiles that are well described by the model [including Eq. (36)]; one case is a "pure" convective mixed layer (i.e., $-L/z_i < 0.1$) while the other case shows considerable surface shear effects (i.e., $-L/z_i > 0.1$). Figure 8 gives two corresponding cases where the model does poorly. The uppermost data point plotted on the profiles is an average value from within the interface where the model of Wyngaard and LeMone (1980) is applicable. The interfacial value predicted by their model is indicated by the open circle. Only twelve C_Q^2 profiles were available. These were compared to the model using

$$R_Q = (\Delta Q/\Delta\theta)(\theta_*/Q_*)R_\theta. \tag{38}$$

The results were similar to the C_T^2 results so they are not shown here.

6. Discussion

The model presented in this paper is intended to represent the behavior of scalar structure function parameters in the entraining, unstable mixed-layer. A top-

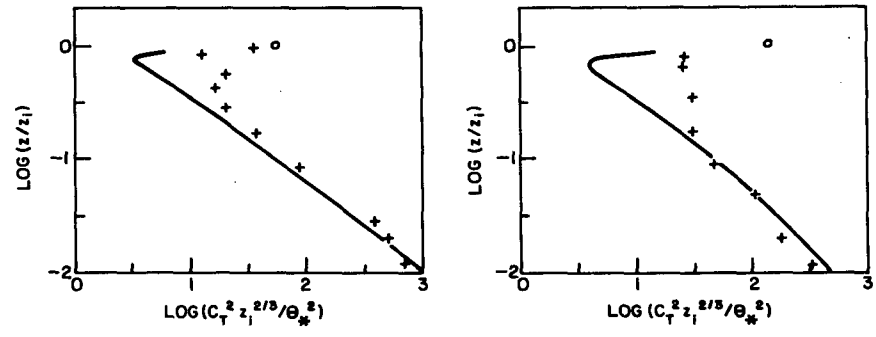

FIG. 8. Similar to Fig. 7. In the left panel is data taken over the Gulf of Mexico near Panama City, FL with an inversion height of 1100 m, $u_* = 0.34$ m s^{-1}, $T_* = -0.49$ K, $R_\theta = -0.21$ and $-L = 15$ m. In the right panel is data taken off the coast of California near Monterey with an inversion height of 360 m, $u_* = 0.28$ m s^{-1}, $T_* = -0.078$ K, $R_\theta = -0.32$ and $-L = 70$ m.

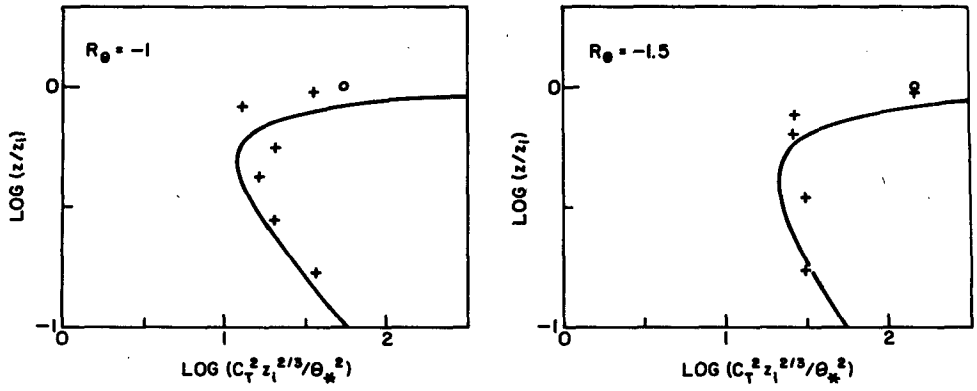

FIG. 9. Similar to Fig. 6 with the same data from Fig. 8. In this case a value of R_θ is selected that gives the best model representation of the data points; the value of R_θ is given in the upper left corner of the panel.

down and bottom-up diffusion approach is used where conventional convective scaling is augmented with an additional scaling parameter, the ratio of entrainment to surface flux of the relevant scalar quantity. The scaling parameters are incorporated into empirical functional relationships that are obtained from large-eddy simulations. Qualitatively, the model is able to produce deviations from the classic convective ($z^{-4/3}$) profile that are quite similar to those observed in the atmosphere. The top-down component of the model is in very good agreement with a set of measurements of C_Q^2 taken under conditions believed to be dominated by the entrainment flux.

However, a comparison with twenty aircraft profiles showed that the model often poorly describes the C_T^2 behavior. A lesser number of C_Q^2 profiles were examined and yielded qualitatively similar results. In fact, only five of the twenty profiles were accurately represented by the model. Typically, the model underpredicted the value of C_T^2, by as much as a factor of 10, for $z/z_i > 0.5$ (e.g., see Fig. 8). Apparently the effects of entrainment are being underestimated in many situations. It is possible that the model is essentially correct but the entrainment rate is much larger than that predicted by Eq. (36). For example, if we select proper values for R_θ, then the model curves can be made to fit the data much more accurately. By way of illustration, the profiles of Fig. 8 have been replotted (Fig. 9) to emphasize the mixed-layer region and a value of R_θ has been found that gives a better fit. It is certainly conceivable that the entrainment rate is higher for many of the profiles. Other entrainment producing mechanisms exist (e.g., inversion wind shear, breaking gravity waves) in cloudfree conditions and, in fact, the measurements were made under fair weather conditions that were not truly cloudfree (the aircraft did not actually enter any clouds while obtaining the profiles but, in many cases, broken clouds were present). A survey of R_θ values that provide the best fit to the twenty profiles finds them roughly evenly distributed from -0.2 to -1.5 with an average of -0.8. Since the average value of R_θ predicted by Eq. (36) is -0.27, this implies a factor of three increase in the entrainment rate. There is at least one good reason why this is an unpalatable increase. The entrainment rate predicted by Eq. (36) is also incorporated in models of the interfacial values of the structure functions. In a previous analysis of these same twenty profiles (Fairall, 1984), the Wyngaard-Lemone interfacial a model was found to agree, on average, with the measurements (the rms scatter was about a factor of 2).

A second possibility is that the entrainment velocity is correct but the effects of entrainment on the temperature structure function are greater in the atmosphere than implied by the large-eddy simulations. This notion finds support in a recent analysis of aircraft measurements of mean scalar gradients near the top of the boundary layer by Lenschow et al. (1985). They found the gradients to be two to four times greater than those predicted by the large eddy simulations. This would imply similarly greater gradient production of variance, and therefore, greater structure function parameters but appears to conflict with the good agreement for the top-down term shown in Fig. 6. A third possibility is that some other aspect of the large eddy simulations is inadequate. Evidence for this can be found in Moeng and Wyngaard's Fig. 11a, where temperature variance from the large eddy simulation is significantly less than atmospheric observations. Wyngaard and Moeng (private communication, 1986) have recently run finer resolution simulations that show a significantly larger gain in the transport terms that would lead to larger values for the structure parameters. Given the nature of the evidence, it is clear that more work must be done to resolve this puzzle.

Acknowledgments. The author wishes to acknowledge discussions with Dennis Thomson, John Wyngaard and Steve Burk. This work was partially supported by the Office of Naval Research (Grant N0014-

85-K-0250) and the Air Force Office of Scientific Research (Grant AFOSR—86-0049).

REFERENCES

Burk, Stephen D., 1981: Comparison of structure parameter scaling expressions with turbulence closure model predictions. *J. Atmos. Sci.*, **38,** 751–761.

Caughey, S. J., and S. G. Palmer, 1979: Some aspects of turbulence structure through the depth of the convective boundary layer. *Quart. J. Roy. Meteor. Soc.*, **105,** 811–827.

Davidson, K. L., T. M. Houlihan, C. W. Fairall and G. E. Schacher, 1978: Observation of the temperature structure parameter, C_T^2, over the ocean. *Bound. Layer Meteor.*, **15,** 507–523.

Druilhet, A., J. P. Frangi, D. Guedalia and J. Fontan, 1983: Experimental studies of the turbulence structure parameters of the convective boundary layer. *J. Climate Appl. Meteor.*, **22,** 594–608.

Dubosclard, G., 1982: A sodar study of the temperature structure parameter in the convective boundary layer. *Bound. Layer Meteor.*, **22,** 325–334.

Fairall, C. W., 1984: Wind shear enhancement of entrainment and refractive index structure parameter at the top of a turbulent mixed layer. *J. Atmos. Sci.*, **41,** 3472–3484.

——, R. Markson, G. E. Schacher and K. L. Davidson, 1980: An aircraft study of turbulence dissipation and temperature structure parameter in the unstable marine atmospheric boundary layer. *Bound. Layer Meteor.*, **19,** 453–469.

Frisch, A. S., and G. R. Ochs, 1975: A note on the behavior of the temperature structure parameter in a convective layer capped by a marine inversion. *J. Appl. Meteor.*, **14,** 415–419.

Kaimal, J. C., J. C. Wyngaard, D. A. Haugen, O. R. Cote, Y. Izumi, S. J. Caughey and C. J. Readings, 1976: Turbulence structure in the convective boundary layer. *J. Atmos. Sci.*, **33,** 2152–2169.

Kohsiek, N., 1982: Measuring C_T^2, C_q^2 and C_{Tq} in the unstable surface layer, and relations to the vertical fluxes of heat and moisture. *Bound. Layer Meteor.*, **24,** 89–107.

Lenschow, D. H., M. Y. Zhou and B. Boba Stankov, 1985: The scalar gradient near the top of the convective boundary layer. *Proc. Eighth Symp. on Turbulence and Diffusion,* Denver, Amer. Meteor. Soc. 67–70.

Moeng, C.-H., and J. C. Wyngaard, 1984: Statistics of conservative scalars in the convective boundary layer. *J. Atmos. Sci.*, **41,** 3162–3169.

Smith, S. D., R. J. Anderson, G. D. Hartog, D. R. Topham and R. G. Perkin, 1983: An investigation of a Polyna in the Canadian Archipelagos, structure of turbulence and heat flux. *J. Geophys. Res.*, **88,** 2900–2910.

Tatarskii, V. I., 1972: *The Effects of the Turbulent Atmosphere on Wave Propagation.* Kefer Press, Jerusalem, 472 pp.

Tennekes, H., and A. G. M. Driedonks, 1981: Basic entrainment equations for the atmospheric boundary layer. *Bound. Layer Meteor.*, **20,** 515–531.

Weill, A., C. Klapisz, B. Strauss, F. Baudin and C. Jaupart, 1980: Measuring heat flux and structure functions of temperature fluctuations with an acoustic doppler sodar. *J. Appl. Meteor.*, **19,** 199–205.

Wyngaard, J. C., 1973: On surface-layer turbulence. *Workshop on Micrometeorology,* D. A. Haugen, Ed., Amer. Meteor. Soc., 101–149.

——, and R. A. Brost, 1984: Top-down and bottom-up diffusion of a scalar in the convective boundary layer. *J. Atmos. Sci.*, **41,** 102–112.

——, and M. A. LeMone, 1980: Behavior of the refractive index structure parameter in the entraining convective boundary layer. *J. Atmos. Sci.*, **35,** 1573–1585.

——, Y. Izumi and S. A. Collins, 1971: Behavior of the refractive index structure parameter near the ground. *J. Opt. Soc. Am.*, **61,** 1646–1650.